NAVAL POSTGRADUATE SCHOOL

MONTEREY, CALIFORNIA

THESIS

A MATHEMATICAL EXPLORATION OF ONE-DIMENSIONAL DEPTH PENETRATION BY ELECTROMAGNETIC WAVES

by

Neal E. Mooers

June 2021

Thesis Advisor:	Hong Zhou
Second Reader:	Anthony Austin

THIS PAGE INTENTIONALLY LEFT BLANK

REPORT DOCUMENTATION PAGE			*Form Approved OMB No. 0704-0188*
Public reporting burden for this collection of information is estimated to average 1 hour per response, including the time for reviewing instruction, searching existing data sources, gathering and maintaining the data needed, and completing and reviewing the collection of information. Send comments regarding this burden estimate or any other aspect of this collection of information, including suggestions for reducing this burden, to Washington headquarters Services, Directorate for Information Operations and Reports, 1215 Jefferson Davis Highway, Suite 1204, Arlington, VA 22202-4302, and to the Office of Management and Budget, Paperwork Reduction Project (0704-0188) Washington, DC 20503.			
1. AGENCY USE ONLY ***(Leave blank)***	**2. REPORT DATE** June 2021	**3. REPORT TYPE AND DATES COVERED** Master's thesis	
4. TITLE AND SUBTITLE A MATHEMATICAL EXPLORATION OF ONE-DIMENSIONAL DEPTH PENETRATION BY ELECTROMAGNETIC WAVES			**5. FUNDING NUMBERS**
6. AUTHOR(S) Neal E. Mooers			
7. PERFORMING ORGANIZATION NAME(S) AND ADDRESS(ES) Naval Postgraduate School Monterey, CA 93943-5000			**8. PERFORMING ORGANIZATION REPORT NUMBER**
9. SPONSORING / MONITORING AGENCY NAME(S) AND ADDRESS(ES) N/A			**10. SPONSORING / MONITORING AGENCY REPORT NUMBER**
11. SUPPLEMENTARY NOTES The views expressed in this thesis are those of the author and do not reflect the official policy or position of the Department of Defense or the U.S. Government.			
12a. DISTRIBUTION / AVAILABILITY STATEMENT Approved for public release. Distribution is unlimited.			**12b. DISTRIBUTION CODE** A

13. ABSTRACT (maximum 200 words)

Electromagnetic pulse (EMP) weapons are widely recognized as a potential disruption to infrastructures that are based on electronic equipment. Use of an EMP platform presents a significant opportunity for aggressive actors to disable infrastructure without causing physical damage to structures or individuals. As more aspects of society depend on electronic controls, passive measures of protection for critical systems will be more valuable for maintaining a viable national security posture. This leads to the natural question: are construction materials and natural materials viable methods to shield sensitive electronics from EMP fields? By discretizing Maxwell's equations for electromagnetics via a finite-difference time-domain method, we can observe the behavior of the electric field as it propagates through various materials to see if they provide adequate protection. From this discretization, we were able to analyze individual material properties to find the best traits for protective measures. We found that the electrical conductivity is the most significant material property that contributes to attenuation of electric fields, with increases in conductivity corresponding to approximate exponential decreases in the magnitude of electric field propagation. After running these simulations, we find that many common construction and natural materials offer significant protection, but electric fields from an EMP could be large enough to penetrate the layer at damaging levels.

14. SUBJECT TERMS electromagnetic pulse, EMP, finite-difference time-domain, Maxwell's equation, numerical solver, attenuation, discretization, conductivity, permittivity, permeability			**15. NUMBER OF PAGES** 67
			16. PRICE CODE
17. SECURITY CLASSIFICATION OF REPORT Unclassified	**18. SECURITY CLASSIFICATION OF THIS PAGE** Unclassified	**19. SECURITY CLASSIFICATION OF ABSTRACT** Unclassified	**20. LIMITATION OF ABSTRACT** UU

THIS PAGE INTENTIONALLY LEFT BLANK

Approved for public release. Distribution is unlimited.

A MATHEMATICAL EXPLORATION OF ONE-DIMENSIONAL DEPTH PENETRATION BY ELECTROMAGNETIC WAVES

Neal E. Mooers
Captain, United States Army
BSCE, Oklahoma State University, 2013

Submitted in partial fulfillment of the
requirements for the degree of

MASTER OF SCIENCE IN APPLIED MATHEMATICS

from the

NAVAL POSTGRADUATE SCHOOL
June 2021

Approved by: Hong Zhou
Advisor

Anthony Austin
Second Reader

Wei Kang
Chair, Department of Applied Mathematics

THIS PAGE INTENTIONALLY LEFT BLANK

ABSTRACT

Electromagnetic pulse (EMP) weapons are widely recognized as a potential disruption to infrastructures that are based on electronic equipment. Use of an EMP platform presents a significant opportunity for aggressive actors to disable infrastructure without causing physical damage to structures or individuals. As more aspects of society depend on electronic controls, passive measures of protection for critical systems will be more valuable for maintaining a viable national security posture. This leads to the natural question: are construction materials and natural materials viable methods to shield sensitive electronics from EMP fields? By discretizing Maxwell's equations for electromagnetics via a finite-difference time-domain method, we can observe the behavior of the electric field as it propagates through various materials to see if they provide adequate protection. From this discretization, we were able to analyze individual material properties to find the best traits for protective measures. We found that the electrical conductivity is the most significant material property that contributes to attenuation of electric fields, with increases in conductivity corresponding to approximate exponential decreases in the magnitude of electric field propagation. After running these simulations, we find that many common construction and natural materials offer significant protection, but electric fields from an EMP could be large enough to penetrate the layer at damaging levels.

THIS PAGE INTENTIONALLY LEFT BLANK

Table of Contents

List of Figures

THIS PAGE INTENTIONALLY LEFT BLANK

List of Tables

THIS PAGE INTENTIONALLY LEFT BLANK

List of Acronyms and Abbreviations

CFL Courant Friedrichs Lewy

E1 HEMP early time high altitude electromagnetic pulse

EMP electromagnetic pulse

FDTD finite difference time domain

HEMP high altitude electromagnetic pulse

HOB height of burst

PEC perfect electric conductor

USG United States government

THIS PAGE INTENTIONALLY LEFT BLANK

Acknowledgments

There have been many people who have made this project a success and too many people to fully thank on a page. That said, there are a few specific people I would like to thank by name.

To my advisor, Dr. Zhou, thank you for involving me in this project early in my time here. I learned a lot about research and refinement under you guidance, and the foundation you helped lay will be paramount to my success going forward.

To my second reader, Dr. Austin, I thank you for your valuable input to this project. Your passion for PDEs and numerical methods was infectious, and the expertise you shared was crucial to my development and success.

To the rest of the faculty and staff, thank you for sharing your wide breadth of knowledge with me. I came to NPS as a casual maths enjoyer, but you have sparked joy in the wide world of mathematics that I didn't even know existed prior to my arrival. I look forward to experiencing the world more fully with this maths-based mindset.

To my cohort, I have enjoyed these past few years sharing the classroom. At one point or another, I have come to each of you to bounce ideas or work through a problem, and each of you has been a tremendous help. I hope to work with each of you in the future.

To my friends and family back home, thank you for your words of encouragement and support during this process. No man is an island, and you have kept me functional.

THIS PAGE INTENTIONALLY LEFT BLANK

CHAPTER 1:
Introduction and Problem Background

1.1 Context

As the United States continually adopts and improves electronically controlled infrastructure in military and civilian realms, the improvements in production come with increased susceptibility to disruption by adversarial forces [1]. A significant threat with potential to damage electrical wiring and control systems is the electromagnetic pulse (EMP), with specific attention paid to the EMP generated by a high altitude electromagnetic pulse (HEMP) burst [2] from a nuclear weapon blast. These hold the potential to cause prolonged damage to electrical systems, which may have cascading effects similar to those observed in 2005 after Hurricane Katrina on a much larger geographic scale [2]. Due to the potential for significant damage to infrastructure and national defense, examination and improvement of national assets has become a priority for U.S. government (USG) officials [3].

1.2 Motivation

Although EMPs present a significant threat to national security, experimental data on them is very limited, which creates gaps in our knowledge [3]. In particular, there is almost no empirical testing data on HEMP due to a 1963 test ban treaty between the USG and the Soviet Union [1]. The early time (E1) effects of HEMP provide a highly concerning threat. This E1 HEMP field would be produced in the first microsecond after a high altitude nuclear blast and generate the largest electric field by far [4], as illustrated in Figure 1.1. This could prevent safety systems from engaging before significant damage from later time HEMP stages [5]. Due to both the wide area effect from a blast at satellite altitude [6] and the available delivery by multiple non-friendly states [1], this EMP delivery mechanism presents a concern to security interests.

1.2.1 History

Although electromagnetic effects were expected in early nuclear tests, the mechanisms were not well understood and the predictions were not highly accurate [4]. Some of the

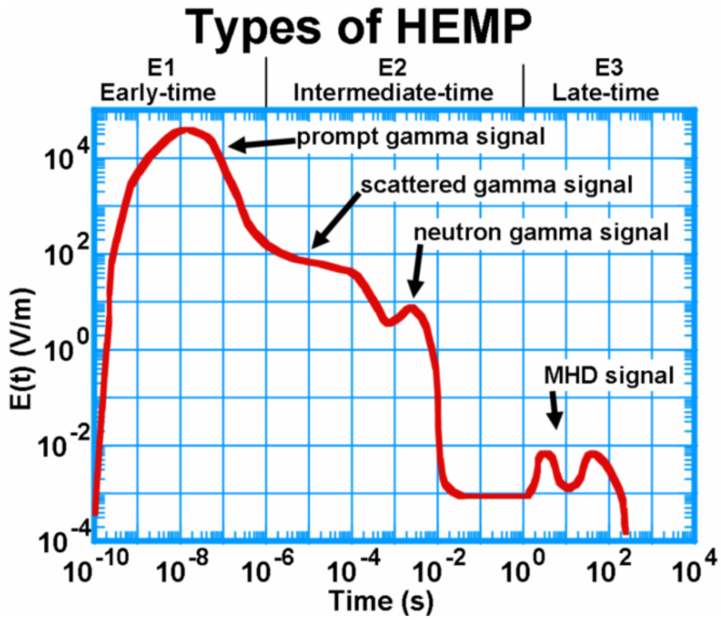

Figure 1.1. Parts of HEMP and maximum values of a generic signal
Source: [4].

earliest observations of EMP effects were during the early 1950s, in the form of what British researchers called radioflash [7]. This and other key events are listed in Table 1.1.

The only instances of deliberate HEMP testing occurred in the 1960s, with both the U.S. and Soviet Union conducting tests in 1962. The most well-known being the U.S. Starfish Prime test at Johnston Atoll, which produced effects over 1400 km away in Hawaii by damaging streetlamps and a few other electrical systems [8]. Due to the lack of understanding of the mechanism of HEMP, the instrumentation on hand was not sufficient to gather quality data, although the data acquired was enough to confirm the presence of E1 HEMP [4]. Models and analysis were conducted afterward to build a model that would reasonably explain HEMP effects, although the true effects of the Starfish Prime test could not be definitively confirmed [9]. Russian tests in 1962 also provided evidence of E1 HEMP effects, with testing related damage occurring in antenna systems and diesel generators [4]. Further empirical testing of HEMP was discontinued in 1963 when the USG and the Soviet Union signed the Limited Test Ban Treaty, effectively ending all full scale testing on E1 HEMP [2]. Due to this lack of empirical data, computer models have been necessary for testing theory.

Table 1.1. Key Events in EMP History
Source: [4]

Year	Event
1945	TRINITY EVENT; electronic equipment shielded reportedly because of Fermi's expectation of EM signals from a nuclear burst
1951	C.H. Papas of LASL proposes prompt gamma-produced Compton currents as sources of EMP
1951-1952	First deliberate EMP observations made by Shuster, Cowan, and Reines
1951-1953	First British atomic tests; instrumentation failures attributed to "radioflash"
1957	Bethe makes estimate of high-altitude EMP signals using electric dipole model (early-time peak incorrect)
1957	Haas makes magnetic field measurements for PLOMBBOB test series (interest in EMP possibly setting off magnetic mines)
1958	Joint British/U.S. meeting begins discussions of system EMP vulnerability and hardness issues
1958	Kampaneets (USSR) publishes open literature paper on EMP from atomic explosion
1959	Pomham and Taylor of the U.K. present a theory of "radioflash"
1962	FISHBOWL high-altitude tests; EMP measurements driven off scale; first-indications of the magnitude of high-altitude EMP signal
1962	SMALL BOY ground burst EMP test
1963	Open literature calls for EMP hardening of military systems begin to appear
1963-1964	First EMP system tests carried out by Air Force Weapons Laboratory (AFWL) (now Air Force Research Laboratory, Directed Energy Directorate)
1963-1964	Longmire gives a series of EMP lectures at AFWL; presents detailed theory of ground burst EMP and shows that the peak of the high-altitude EMP signals is explained by magnetic field turning (magnetic dipole signal)
1964	First note in the LASL/AFWL EMP notes series published
1965	Karzas and Latter publish first open literature paper giving high-frequency approximation for the high-altitude magnetic dipole signal
1967	Construction of ALECS as the first guided-wave simulator is completed for EMP simulation on missiles
1967	AJAX underground nuclear test
1969	Close-in EMP mechanisms recognized and evaluated by Graham and Schaefer
1970	EMP underground test feasibility recognized and preliminary design presented by Schaefer
1973	First joint nuclear EMP meeting at AFWL
1974	MING BLADE underground EMP test for confirmation of near surface burst EMP models
1975	DINING CAR underground EMP test as the first system hardware EMP test

1.2.2 Susceptibility

Due to advances in technology and the lack of testing, the actual effects of E1 HEMP on modern electronics is still poorly understood [2]. The effects of HEMP have only been observed in vacuum tube systems, which are on the order of 10 million times more resistant than modern circuit systems [10]. Further testing has been conducted using underground nuclear blasts [7] which have improved the understanding of the associated physics, but has not yielded comparably valuable information about effects on equipment. The current threat assessment expects communication equipment to be the most affected set of technology [10]. Deliberate protection measures have been developed and constructed, most notably the Faraday cage, but are not 100% effective at disrupting electromagnetic waves [11].

1.3 Roadmap

This thesis will examine the effects of E1 HEMP by numerically simulating depth penetration of the electrical and magnetic fields from the EMP generating event. Chapter 2 looks at previous work and the basis for the mathematical model that describe the propagation of EMP waves. Chapter 3 derives and implements the equations that govern the propagation through media. Chapter 4 summarizes and shows the results obtained through our implementation and analyzes the effects of varying the input parameters. Finally, Chapter 5 presents conclusions and potential directions of future work. The code used to generate the data is included in the Appendix.

CHAPTER 2:
Previous Work Analysis

2.1 Previous Works

The related previous work can be divided into two categories: analysis of HEMP and analysis of Maxwell's equations. Each of these categories has multiple components that were examined in this review.

2.1.1 High Altitude Electromagnetic Pulse

Specific data on the effects of a HEMP blast are not readily available to the public as the details from the generating events would require disclosure of classified weapons platforms [2]. As such, publicly available studies cover either approximation of EMP environments or infrastructure susceptibility.

A key base for unclassified analysis of HEMP environments was provided by Oak Ridge National Laboratory [12]. In this report, the team analyzed a nominal 3.3 megaton nuclear burst above the atmosphere. Specifically, they studied the peak electric field values at various geographic points within line of sight of a burst. Using early computer algorithms, they found nominal values based on a specific burst location and specific radii from the epicenter. These results aligned with other work calculating maximum detection distance for high altitude nuclear explosions [13].

From these simulations, they found a nominal warhead could generate a peak electric field on the order of 5 times $10^5 \frac{V}{m}$ at the peak below the blast with decreasing magnitude further from the blast [12]. This peak electric field was for the E1 HEMP value, which occurs in the first few μs after the blast as seen in Fig 1.1. In retroactive analysis of the Starfish Prime event, the peak electric fields were calculated to be significant enough to have caused damage in Honolulu, as the EMP induced electric field caused street light bulbs to go out [9].

Other documents provide a strong overview of the effects of E1 HEMP in relation to U.S. susceptibility. These documents provide nominal values for generic blasts and the relationship between height of burst (HOB) and radius of effect [4]. This work indicates that a single burst at 400 km HOB will cover a 2400 km radius, enough to cover most of the contiguous U.S. It also calculates the relative effects to other EM methods, including FM. These works discuss qualitative and approximate effects on electronics and potential area of effect, with the conclusion that a single blast could feasibly affect the entire U.S. [14]. This is illustrated in Figure 2.1, which illustrates the effect from a low yield weapon at a relatively low altitude of 75 km above the middle of the country.

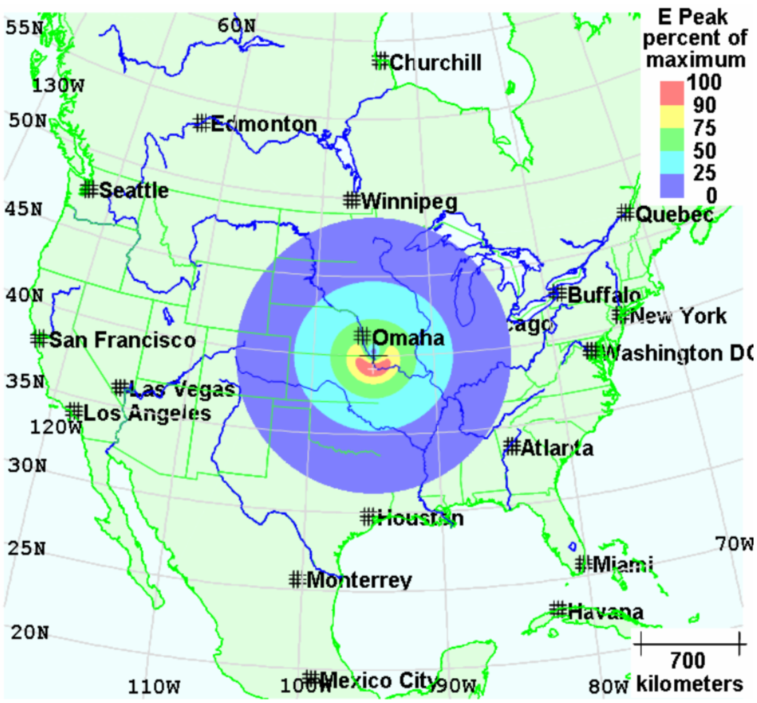

Figure 2.1. Map illustrating magnitude of E1 electric field from HEMP detonated 75 km above the central U.S. Source: [4].

2.1.2 Maxwell's Equations

Maxwell's equations have been analyzed both analytically and numerically. The numerical solutions are discretizations of the analytic formulations and used more frequently due to advances in computation power [15], especially in situations where the analytic solution is not easily solvable.

Evaluation Methods

The relationship between electric and magnetic fields are described by Maxwell's equations, a set of differential equations that relate Faraday's, Ampere's, and Gauss's laws [16]. These equations serve as the basis for current studies in electromagnetics. These equations are well understood in their analytic form, having been separated into Cartesian components [17] for directional analysis.

Early methods of solving Maxwell's equations focused on the frequency domain [15] for steady-state problems, as it offers a closed form solution that was solvable on early calculating devices. During the early implementation of modern computers, more advanced frequency domain solutions were used, although they reached their limits due to sizes of problem sets and their poor fit with non-metallic objects. This led to the rise of time domain solving techniques.

There have been commercial software implementations for Maxwell's equations either produced by companies or implemented on their platforms. COMSOL has developed a finite element method solver based on proprietary code that they sell for evaluation of electromagnetic waves in various objects [18]. Additionally, there are MATLAB finite difference algorithms published [19], although the specific implementation relies on induced fields inside a space rather than a field entering a space.

Finite Difference

A popular numerical method for solving Maxwell's equations is the finite-difference time domain (FDTD) method, which focuses on numerically solving spatial values at various time steps. This technique was first employed by Yee to find solutions to electromagnetic problems without closed form solutions [20], offering a numerical approach to solve the system of partial differential equations. Yee's method relied on building a grid where each spatial point is influenced by its previous value and the values at neighboring points offset by half steps in space and time and is shown in Figure 2.2. The technique was expanded to complicated structures in three-dimensional Cartesian space [21] and eventual employment in spherical coordinates [22]. The spherical coordinates offered some improvement over Cartesian space, although it was more apt to lose stability at the boundaries for large problems.

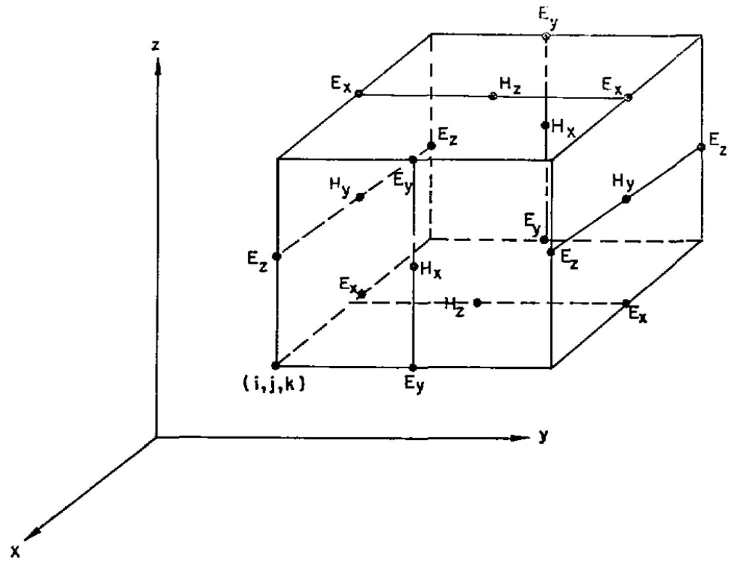

Figure 2.2. Rectangular coordinate representation of the Yee grid, which shows the relationship between electric fields on boundary lines and magnetic fields on faces. Source: [20].

The FDTD method's stability is dependent on viable spatial and time steps that ensure accuracy is not lost at each step. This was previously formulated and bounded by Courant et al. [23] for Maxwell's equations. Their method develops bounds to the differential equation so that the wave does not pass any spatial step without evaluation in a single time step. This means the spatial step has to be less than the time step divided by wave propagation rate, a requirement known as the Courant-Freidrichs-Lewy (CFL) condition for differential equations. Additional key events in the expansion of FDTD methods can be seen in Table 2.1.

2.2 Gaps in Analysis

Though many of the individual elements have been analyzed, there is very little available literature on depth penetration of an EMP. Specifically, there is little available describing passive protective measures against an E1 HEMP attack. The effect on material selection and thickness variation on EMP attenuation is a current knowledge gap.

Table 2.1. Partial History of FDTD
Adapted from [15].

Key Events in FDTD	
Year	Paper
1966	Yee describes the basis for the FDTD method
1975	Taflove and Brodwin confirm numerical stability criterion
1980	Taflove coined term FDTD and published model of 3-D penetration to metal cavity
1987,90	Finite Element Time Domain (FETD) and Finite Volume Time Domain (FVTD) methods introduced Cangellaris et al., and Shankar et al.
2000	Rylander and Bondeson introduced a stable, hybrid FDTD-FE technique
2003	DeRaedt introduced unconditionally stable one-step FDTD technique

THIS PAGE INTENTIONALLY LEFT BLANK

CHAPTER 3:
Methodology and Model

3.1 Solving Technique

To conduct EMP wave penetration analysis, we use the FDTD technique to analyze Maxwell's equations in various media. We choose this method as it provides relatively simple formulations for handling anisotropic dielectric materials (i.e., those having differing property values when measured in differing directions) and those that vary along their geometry. In order to do this, we use a discretization technique on the differential forms of Maxwell's equations. This discretization works by taking the known value from solving at a starting time for every point and taking a small step to solve for the values at every location at the next time step. In setting up this evaluation, the problem space is modeled such that a wave propagates in one-dimension with field values existing in the two other spatial dimensions. The space is developed so that a modeled EMP wave will enter the space, attenuate, and exit the space. The behavior in the attenuation portion is of key interest in this problem.

3.2 Algorithm Derivation

In order to make the calculations for the EMP penetration, the correct derivation of Maxwell's equations must be found and then be discretized effectively. The goal is to take distinct, finite steps in the temporal and spatial dimensions to solve for specific times and spaces, rather than a closed form solution for the field strength at arbitrary times and locations. This is accomplished first by rearranging Maxwell's equations to a usage form, and second by numerically placing them into the one-dimensional Yee grid so that it can be implemented by a computer algorithm.

3.2.1 Maxwell's Equations

To begin, the proper implementation of Maxwell's equations was derived for implementation. The common represented starting point is given as [24], [19]:

$$\nabla \times \vec{H} - \frac{\partial \vec{D}}{\partial t} = \vec{J} \tag{3.1a}$$

$$\nabla \times \vec{E} + \frac{\partial \vec{B}}{\partial t} = -\vec{M} \tag{3.1b}$$

$$\nabla \cdot \vec{D} = \rho_e \tag{3.1c}$$

$$\nabla \cdot \vec{B} = \rho_m \tag{3.1d}$$

where

- $\vec{H}$ is the magnetic field
- $\vec{E}$ is the electric field
- $\vec{D}$ is the electric displacement
- $\vec{B}$ is the magnetic flux density
- $\vec{J}$ is the electric current density
- $\vec{M}$ is the magnetic current density
- ρ_e is the electric charge density
- ρ_m is the magnetic charge density

Using the definitions [19]:

$$\vec{D} = \varepsilon \vec{E} \tag{3.2a}$$

$$\vec{B} = \mu \vec{H} \tag{3.2b}$$

and plugging into (3.1), Maxwell's equations are now represented as:

$$\nabla \times \vec{H} = \varepsilon \frac{\partial \vec{E}}{\partial t} + \vec{J} \tag{3.3a}$$

$$\nabla \times \vec{E} = \mu \frac{\partial \vec{H}}{\partial t} - \vec{M} \tag{3.3b}$$

$$\nabla \cdot \varepsilon \vec{E} = \rho_e \tag{3.3c}$$

$$\nabla \cdot \mu \vec{H} = \rho_m \tag{3.3d}$$

where

- ε is the permittivity
- μ is the permeability

In common representation, $\varepsilon = \varepsilon_0 \varepsilon_r$, which represents the permittivity of a space as the permittivity of free space times the relative permittivity. We take $\varepsilon_0 \approx 8.854 \times 10^{-12} \frac{F}{m}$. Similarly, $\mu = \mu_0 \mu_r$, where $\mu_0 = 4\pi \times 10^{-7} \frac{H}{m}$.

The electric and magnetic current densities can each be separated into the conduction and impressed current densities, [19]:

$$\vec{J} = \vec{J}_c + \vec{J}_i \tag{3.4a}$$

$$\vec{J}_c = \sigma^e \vec{E} \tag{3.4b}$$

$$\vec{M} = \vec{M}_c + \vec{M}_i \tag{3.4c}$$

$$\vec{M}_c = \sigma^m \vec{H} \tag{3.4d}$$

where

- σ^e is the electric conductivity
- σ^m is the magnetic conductivity
- J_c is the conduction current density
- J_i is the impressed current density
- M_c is the conduction magnetic density

- M_i is the impressed magnetic density

The two divergence equations, (3.3c) and (3.3d), are not used in the development of the FDTD equations [19], but can be used to verify the results obtained from derivation using the two curl equations, (3.3a) and (3.3b). Plugging in the equivalencies for the electric and magnetic current densities updates the representation of Maxwell's equations to:

$$\nabla \times \vec{H} = \varepsilon \frac{\partial \vec{E}}{\partial t} + \sigma^e \vec{E} + \vec{J}_i \tag{3.5a}$$

$$\nabla \times \vec{E} = -\mu \frac{\partial \vec{H}}{\partial t} - \sigma^m \vec{H} - \vec{M}_i \tag{3.5b}$$

For each material property in (3.5), there exists a direction component and potential variation across the material. This means the material could have differing values for any property ε, μ, σ^e, or σ^m in each of the i, j, and k planes. Further, each material can vary with positionally. This set of equations is valid for any combination of materials, assuming the values for each property are modeled correctly. Each of these properties generalize appropriately and were considered during discretization.

Using the definition of the curl of an equation [25], the original curl can be expanded as:

$$\nabla \times \vec{H} = \left(\frac{\partial H_3}{\partial y} - \frac{\partial H_2}{\partial z}\right)\vec{i} + \left(\frac{\partial H_1}{\partial z} - \frac{\partial H_3}{\partial x}\right)\vec{j} + \left(\frac{\partial H_2}{\partial x} - \frac{\partial H_1}{\partial y}\right)\vec{k} \tag{3.6a}$$

$$\nabla \times \vec{E} = \left(\frac{\partial E_3}{\partial y} - \frac{\partial E_2}{\partial z}\right)\vec{i} + \left(\frac{\partial E_1}{\partial z} - \frac{\partial E_3}{\partial x}\right)\vec{j} + \left(\frac{\partial E_2}{\partial x} - \frac{\partial E_1}{\partial y}\right)\vec{k} \tag{3.6b}$$

which allows solving for each of the directional components. To do this, set each direction from (3.6) to the component in (3.5). This can be done across all six direction components without loss of generality to be:

$$\frac{\partial H_3}{\partial y} - \frac{\partial H_2}{\partial z} = \varepsilon_1 \frac{\partial E_1}{\partial t} + \sigma_1^e E_1 + J_{i1} \tag{3.7}$$

which simplifies to

$$\frac{\partial E_1}{\partial t} = \frac{1}{\varepsilon_1}\left(\frac{\partial H_3}{\partial y} - \frac{\partial H_2}{\partial z} - \sigma_1^e E_1 - J_{i1}\right) \tag{3.8}$$

Upon applying the above calculation to all the directional components, the fields can be written as:

$$\frac{\partial E_1}{\partial t} = \frac{1}{\varepsilon_1}\left(\frac{\partial H_3}{\partial y} - \frac{\partial H_2}{\partial z} - \sigma_1^e E_1 - J_{i1}\right) \tag{3.9a}$$
$$\frac{\partial E_2}{\partial t} = \frac{1}{\varepsilon_2}\left(\frac{\partial H_1}{\partial z} - \frac{\partial H_3}{\partial x} - \sigma_2^e E_2 - J_{i2}\right) \tag{3.9b}$$
$$\frac{\partial E_3}{\partial t} = \frac{1}{\varepsilon_3}\left(\frac{\partial H_2}{\partial x} - \frac{\partial H_1}{\partial y} - \sigma_3^e E_3 - J_{i3}\right) \tag{3.9c}$$
$$\frac{\partial H_1}{\partial t} = \frac{1}{\mu_1}\left(\frac{\partial E_2}{\partial z} - \frac{\partial E_3}{\partial y} - \sigma_1^m H_1 - M_{i1}\right) \tag{3.9d}$$
$$\frac{\partial H_2}{\partial t} = \frac{1}{\mu_2}\left(\frac{\partial E_3}{\partial x} - \frac{\partial E_1}{\partial z} - \sigma_2^m H_2 - M_{i2}\right) \tag{3.9e}$$
$$\frac{\partial H_3}{\partial t} = \frac{1}{\mu_3}\left(\frac{\partial E_1}{\partial y} - \frac{\partial E_2}{\partial x} - \sigma_3^m H_3 - M_{i3}\right) \tag{3.9f}$$

Since we only consider the 1-D case, we don't use the terms that depend on y and z direction movement (i.e., there no variation in y and z directions). An additional consideration is that $M_i = 0$ since there is not a physical meaning for this term in wave propagation [26].

$$\frac{\partial E_1}{\partial t} = \frac{1}{\varepsilon_1}\left(-\sigma_1^e E_1 - J_{i1}\right) \tag{3.10a}$$

$$\frac{\partial E_2}{\partial t} = \frac{1}{\varepsilon_2}\left(-\frac{\partial H_3}{\partial x} - \sigma_2^e E_2 - J_{i2}\right) \tag{3.10b}$$

$$\frac{\partial E_3}{\partial t} = \frac{1}{\varepsilon_3}\left(\frac{\partial H_2}{\partial x} - \sigma_3^e E_3 - J_{i3}\right) \tag{3.10c}$$

$$\frac{\partial H_1}{\partial t} = \frac{1}{\mu_1}\left(-\sigma_1^m H_1\right) \tag{3.10d}$$

$$\frac{\partial H_2}{\partial t} = \frac{1}{\mu_2}\left(\frac{\partial E_3}{\partial x} - \sigma_2^m H_2\right) \tag{3.10e}$$

$$\frac{\partial H_3}{\partial t} = \frac{1}{\mu_3}\left(-\frac{\partial E_2}{\partial x} - \sigma_3^m H_3\right) \tag{3.10f}$$

Two trends are readily apparent from the derivations. The first is the lack of propagation through space for the E_1 and H_1 fields from (3.10a) and (3.10d). Both vary with time, but have no spatial derivative terms meaning there is no propagation through space in the one-dimensional case. This means that at any location away from the source the value of the field in that direction is zero. The only propagating fields are the transverse fields to the direction of travel. The second key is the coupled nature of the electric and magnetic fields. The E_3(3.10c) and H_2(3.10e) fields are completely decoupled from (3.10b) and (3.10f), allowing for update based only on calculated E_3 and H_2 values.

3.2.2 Finite Difference Discretization

For discretizing in one-dimension, a modified Yee grid is established for offsetting the time and spatial dimensions of the electric and magnetic fields. For the temporal offset, the magnetic field update is shifted $\frac{1}{2}\Delta t$ from the electric field update. This is seen in 3.1, where at spatial position (i), the magnetic field update occurs at the time midpoint between each electric field update. This technique is sometimes known as a leapfrog scheme [27] for updating in time.

For the spatial offset, the three-dimensional model is simplified to a single dimension of wave travel. At the time n each electric field acts at the spatial location (i) and the magnetic field at (i) occurs at the midpoint of the space between (i) and $(i + 1)$. This is from

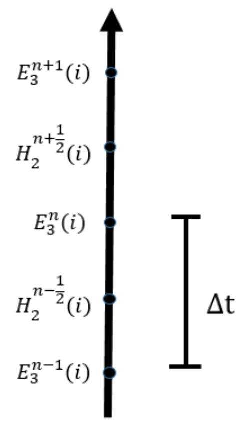

Figure 3.1. Time Discretization of E and H Fields

collapsing the three-dimensional model down, where the electric field updated at vertices and the magnetic field updated at the center of faces. This is illustrated in 3.2, with magnetic field components bordered on each side by electric field components and vice-versa.

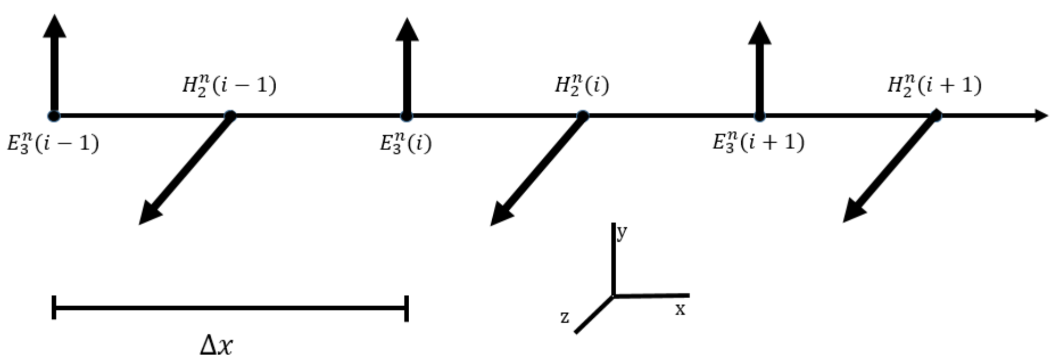

Figure 3.2. Spatial Discretization of E and H Fields

The techniques for derivation will be the same for both the E_3 and H_2 propagation, so the specific equation manipulation will only be shown for E_3.

$$\frac{\partial E_3}{\partial t} = \frac{1}{\varepsilon_3}\left(\frac{\partial H_2}{\partial x} - \sigma_3^e E_3 - J_{i3}\right) \tag{3.11}$$

By replacing the derivatives with finite differences and using a linear interpolation in t to move E_3 to the $n + \frac{1}{2}$ time step, the formulation becomes:

$$\frac{E_3^{n+1}(i)-E_3^n(i)}{\Delta t} = \frac{1}{\varepsilon_3}\left(\frac{H_2^{n+\frac{1}{2}}(i)-H_2^{n+\frac{1}{2}}(i-1)}{\Delta x} - \sigma_3^e(i)\frac{E_3^n(i)+E_3^{n+1}(i)}{2} - J_{i3}^{n+\frac{1}{2}}\right) \tag{3.12}$$

By moving like terms together and factoring out common values, the equation is simplified to:

$$\begin{aligned}(\tfrac{1}{\Delta t} + \tfrac{\sigma_3^e(i)}{2\varepsilon_3(i)})E_3^{n+1}(i) = (\tfrac{1}{\Delta t} - \tfrac{\sigma_3^e(i)}{2\varepsilon_3(i)})E_3^n(i) + \tfrac{1}{\Delta x\varepsilon_3(i)}(H_2^{n+\frac{1}{2}}(i) - H_2^{n+\frac{1}{2}}(i-1)) \\ -\tfrac{1}{\varepsilon_3(i)}J_{i3}^{n+\frac{1}{2}}(i)\end{aligned} \tag{3.13}$$

By isolating the E_3^{n+1} term and applying this technique to H_2, this brings the final set of equations to:

$$\begin{aligned}E_3^{n+1}(i) = \tfrac{2\varepsilon_3(i)-\Delta t\sigma_3^e(i)}{2\varepsilon_3(i)+\Delta t\sigma_3^e(i)}E_3^n(i) + \tfrac{2\Delta t}{2\Delta x\varepsilon_3(i)+\Delta x\Delta t\sigma_1^e(i)}(H_2^{n+\frac{1}{2}}(i) - H_2^{n+\frac{1}{2}}(i-1)) \\ -\tfrac{2\Delta t}{2\varepsilon_3(i)+\Delta t\sigma_3^e(i)}J_{i3}^{n+\frac{1}{2}}(i)\end{aligned} \tag{3.14a}$$

$$H_2^{n+\frac{1}{2}}(i) = \tfrac{2\mu_2(i)-\Delta t\sigma_2^m(i)}{2\mu_2(i)+\Delta t\sigma_2^m(i)}H_2^{n-\frac{1}{2}}(i) + \tfrac{2\Delta t}{2\Delta x\mu_2(i)+\Delta x\Delta t\sigma_2^m(i)}(E_3^n(i+1) - E_3^n(i)) \tag{3.14b}$$

The variables $\varepsilon(i), \mu(i), \sigma^e(i), \sigma^m(i), \Delta t$, and Δx are constant in any media for any specified location (i), these variables can be treated as constant coefficients and simplify the representation of the equations to:

$$E_3^{n+1}(i) = c_{e1}E_3^n(i) + c_{e2}(H_2^{n+\frac{1}{2}}(i) - H_2^{n+\frac{1}{2}}(i-1)) - c_{e3}J_{i3}^{n+\frac{1}{2}}(i) \tag{3.15a}$$

$$H_2^{n+\frac{1}{2}}(i) = c_{h1}H_2^{n-\frac{1}{2}}(i) + c_{h2}(E_3^n(i+1) - E_3^n(i)) \tag{3.15b}$$

where the electrical and magnetic coefficients calculated as:

$$c_{e1} = \frac{2\varepsilon_3(i) - \Delta t \sigma_3^e(i)}{2\varepsilon_3(i) + \Delta t \sigma_3^e(i)} \tag{3.16a}$$

$$c_{e2} = \frac{2\Delta t}{2\Delta x \varepsilon_3(i) + \Delta x \Delta t \sigma_1^e(i)} \tag{3.16b}$$

$$c_{e3} = \frac{2\Delta t}{2\varepsilon_3(i) + \Delta t \sigma_3^e} \tag{3.16c}$$

$$c_{h1} = \frac{2\mu_2(i) - \Delta t \sigma_2^m(i)}{2\mu_2(i) + \Delta t \sigma_2^m(i)} \tag{3.16d}$$

$$c_{h2} = \frac{2\Delta t}{2\Delta x \mu_2(i) + \Delta x \Delta t \sigma_2^m(i)} \tag{3.16e}$$

3.2.3 Error Bounds

The finite difference method has an error bound of on the order of the square of the spatial difference [19]. This $O((\Delta x)^2)$ accuracy is due to the use of the central difference definition of a derivative. This error is obtained using the Taylor series expansion of a function $f(x+h)$ and $f(x-h)$ and adding them. The Taylor series expansion of $f(x+h)$ is [28]

$$f(x+h) = f(x) + hf'(x) + \frac{h^2}{2!}f''(x) + \frac{h^3}{3!}f^{(3)}(x) + \ldots \tag{3.17}$$

and

$$f(x-h) = f(x) - hf'(x) + \frac{h^2}{2!}f''(x) - \frac{h^3}{3!}f^{(3)}(x) + \ldots \tag{3.18}$$

Subtracting (3.18) from (3.17) gives

$$\begin{aligned} f(x+h) - f(x-h) = {} & f(x) + hf'(x) + \frac{h^2}{2!}f''(x) + \frac{h^3}{3!}f^{(3)}(x) + \ldots \\ & - f(x) + hf'(x) - \frac{h^2}{2!}f''(x) + \frac{h^3}{3!}f^{(3)}(x) + \ldots \end{aligned} \tag{3.19}$$

which comes to

$$f(x+h) - f(x-h) = 2hf'(x) + \frac{2h^3}{3!} f^{(3)}(x) + \ldots \tag{3.20}$$

By rearranging and solving for $f'(x)$, the equation for the first derivative of $f(x)$ becomes

$$f'(x) = \frac{f(x+h) - f(x-h)}{2h} + \frac{2h^2}{3!} f^{(3)}(x) + \ldots \tag{3.21}$$

When this is expressed in the final central difference form, the equation is

$$f'(x) = \frac{f(x+h) - f(x-h)}{2h} + O(h^2) \tag{3.22}$$

This expansion shows that the error on the derivative term of the FDTD discretization is a function of Δx, and that using a central difference definition for the derivative puts the error on the order of the spatial difference squared. By selecting a Δx that meets desired accuracy, an appropriate value of Δt can be found that meets the CFL criterion.

3.3 Code Development

Some techniques for this code were modeled after a MATLAB code from [19], which implements FDTD for Maxwell's equations by inducing a current in a vacuum between two perfect electric conductor (PEC) plates. The induction creates two waves propagating in opposite directions along the x-axis until they reflect off the PEC plates at the boundary and return with an equal magnitude wave of opposite sign. This setup allows the analysis of waves reflecting and attenuating in an enclosed space. A visualization of the model code can be seen in Figure 3.3 where we see two equal waves propagating in opposite directions toward PEC plates at the boundary.

In order to increase accessibility and usability of this analysis, the implementation was built in the open-source language Python using the numpy package. However, these techniques are not exclusive to Python and can be implemented in any mathematical computing language.

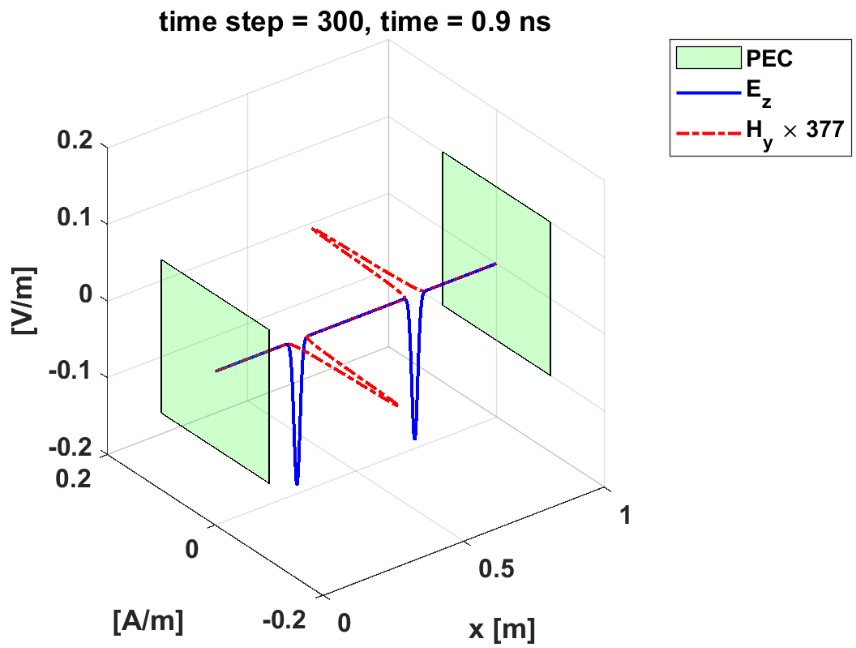

Figure 3.3. Visual Example of Model Code

To implement this algorithm, this code uses one-dimensional arrays to model the spatial aspect of both the electric field, E, and the magnetic field, H. The E-field is discretized using $\frac{depth}{\Delta x} + 1$ nodes to represent the entire depth of the material and the H-field is discretized with $\frac{depth}{\Delta x}$ nodes that represented the space between each E-field node as explained in (3.15). By building the arrays this way, each element of the array represents the fields spaced at intervals of Δx. The bounds for this version are more in line with an EMP entering a space and passing through rather than being enclosed and reflected in a space.

To apply the electric field to the space, a Gaussian waveform function, seen in Figure 3.4, was used to simulate the front edge of the approaching electric field and applied to the first E-field element. This waveform is of the form:

$$W = Ae^{-(\frac{t-a}{b})^n} \tag{3.23}$$

where

- A is the magnitude of the initial field

- t is the time step index
- a and b are EM wave properties provided by [19]
- n controls the shape of the waveform (larger value makes the wave peak wider)

Specifically, the values of n were 2 for Gaussian, 1 for sub-Gaussian, and 10 for super-Gaussian in Figure 3.4. The other values were held constant to the values used later in the implementation of the algorithm for testing.

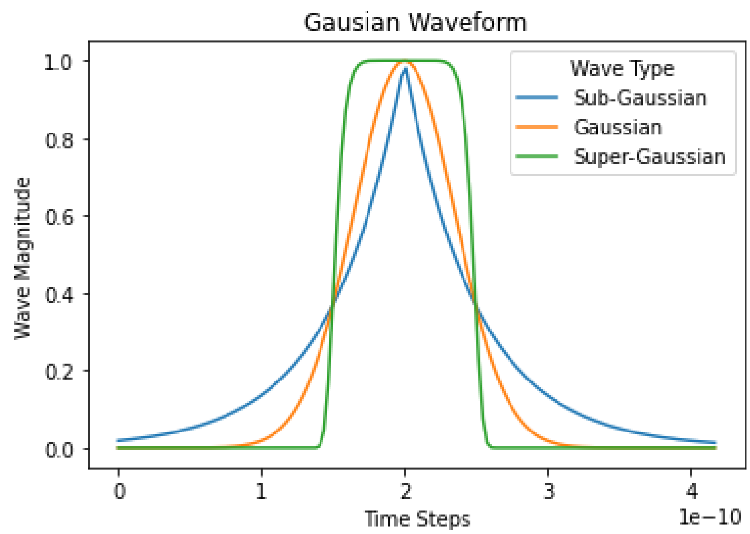

Figure 3.4. Shape of Gaussian Waveforms

Over each time step, the update formula from (3.15) is applied to the H-field at time $n + \frac{1}{2}$, which is then used to update the E-field at time $n + 1$. Finally, the value at the boundary is updated in accordance with the Gaussian wave applied as the incoming wave for each time step. The boundaries for this implementation are not used, as the waveform simulates the field that enters the space and the simulation stops as the wave exits the material of interest, demonstrated in Figure 3.5. By implementing this over arrays and looping through time, the complexity of this operation is $O(nt)$ where n is the size of the field arrays and t is the number of time steps.

To determine the applicable sizes of Δx and Δt, the CFL equation for one-dimensional propagation from [19] can be used to form boundaries. The equation

$$v\Delta t \leq \Delta x \tag{3.24}$$

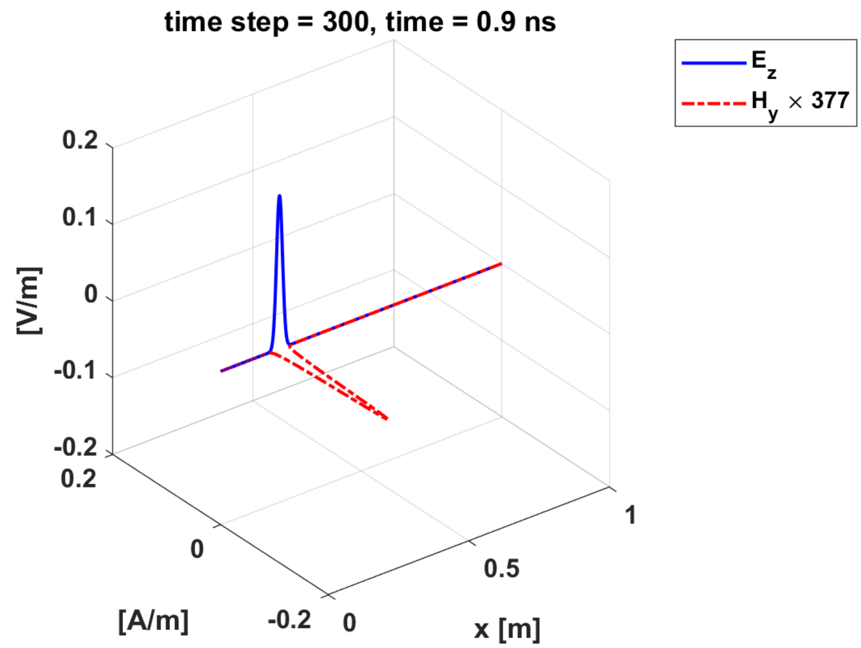

Figure 3.5. Visual Example of Modified Code

gives the relationship between the time and distance differences. With v representing the speed of the wave, the speed of light is used as an upper bound on the potential speed of an electromagnetic wave at $c \approx 3 \times 10^8 \frac{m}{s}$. After rearranging the values, the relationship between Δt and Δx becomes:

$$\frac{\Delta x}{\Delta t} \geq 3 \times 10^8 \frac{m}{s} \tag{3.25}$$

which gives a bound on the ratio of spatial and temporal steps in free space. The speed of light represents a lower bound for this ratio in free space, but a smaller ratio can be used for materials with slower wave propagation.

The technique also allows for approximation of the depth penetration of the peak E-field values for the specified material by using the equation to calculate the speed of electromagnetic waves in a medium [29]. By using the equation

$$v = \frac{1}{\sqrt{\varepsilon\mu}} \tag{3.26}$$

with the values ε and μ for the specific material, the algorithm run time can be adjusted to test various materials for effectiveness at reducing the field at various depths.

In order to perform analysis on realistic materials, Table 3.1 gives values of ε_r, μ_r, and σ^e for various known naturally occurring and construction materials. Due to the fact the system examines propagation in non-magnetic materials, σ^m is not observed and set to zero for calculations [30].

Table 3.1. Electromagnetic Properties of Materials
Adapted from [31], [32], [33], [34], [35], [36], [37], [38], [39], [40].

Material Properties			
Material	Relative Permittivity (ε_r)	Relative Permeability (μ_r)	Electric Conductivity (σ^e)
Air	1.03	1	$\approx 5 \times 10^{-15}$
Wood (Moist)	2	1	$10^{-4} - 10^{-3}$
Wood (Dry)	2	1	$10^{-16} - 10^{-14}$
Water (20°C)	80.2	1	$5 \times 10^{-4} - 5 \times 10^{-2}$
Sea Water (20°C)	73	1	4.8
Sand (Dry)	3 - 6	1 - 1.01	$\approx .008$
Sand (Wet)	20-30	1 - 1.01	$\approx .01$
Clay	5 - 40	1	$.3 - 6 \times 10^{-3}$
Rocky Soil	7	1	$\approx .001$
Limestone	6	1.01	$.2 - 1 \times 10^{-3}$
Sandy Soil (Dry)	3	1	$\approx .006$
Sandy Soil (Wet)	5-17	1	$\approx .008$
Concrete	4.5	2 - 10	$\approx .01 - .2$

CHAPTER 4:
Results and Analysis

To test this implementation, multiple variations of the experiment were analyzed. These tests are based on a generic magnitude of electric field entering the material and then begin to attenuate, as opposed to the magnitude of the field generated by a source. This allows for analysis of material effects on attenuation rather than other interactions related to propagation. Specifically, all tests will look at the trends using a wave load of $10^4 \frac{V}{m}$, which is on the order of magnitude of calculated values from previous experiments [12]. Outputs follow the trends of the electric field magnitude, as these have been demonstrated to be the driver for damage to systems [9]. Unless otherwise specified, the algorithm's spatial and temporal were set to $\Delta x = 1$mm and $\Delta t = 3$ps, the exponent of the Gaussian waveform is 2, and the depth is 1m.

4.1 Tuning Material Parameters

In order to test the material parameters, three sets of variables were modified. The base case considered is the propagation in a free-space scenario, where the values of ε_r and $\mu_r = 1$ and the value of $\sigma^e = 0$. This case causes very little degradation of the field, and peak values are within 99.95% of the original field strength after 1000mm. Subsequently, each parameter was modified in across a range of values for typical construction materials as found in Table 3.1. This allowed us to analyze the influence each parameter has on wave attenuation within the overall system.

As seen in Figure 4.1, we see that the increasing electrical conductivity values significantly alters the magnitude of the electric field at full depth. It has the highest impact of the material parameters, as it is the only parameter tested that can cause > 90% attenuation over the tested depth for values found in Table 3.1. We observe relatively little improvement at early increases, but each order of magnitude increase in σ results in a faster attenuation rate. The solution to a traveling plane wave is expected to be an exponential with a negative exponent [41], so this behavior is in line with expectation.

When examining the permittivity variation, as seen in Figure 4.2, variable increases will

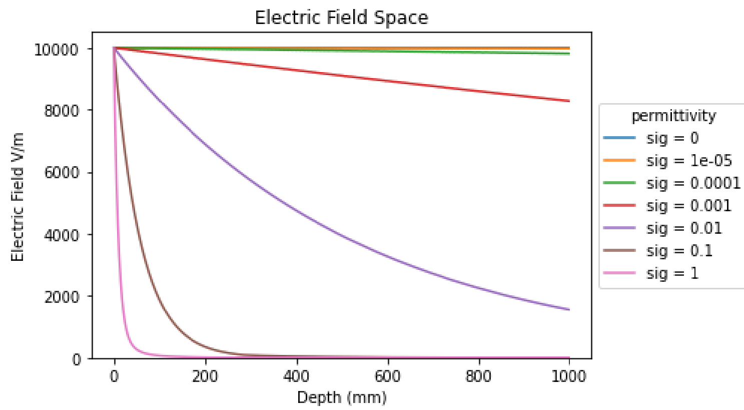

Figure 4.1. Tuning Electrical Conductivity Values with Static ε_r = 1 and μ_r = 1 (1000 mm)

attenuate the field at depth but not to the degree of the conductivity. Over the tested depth of 1m, we saw attenuation of the electric field of approximately 11% at $\varepsilon = 5$ and doubling the attenuation for each subsequent doubling of the ε value.

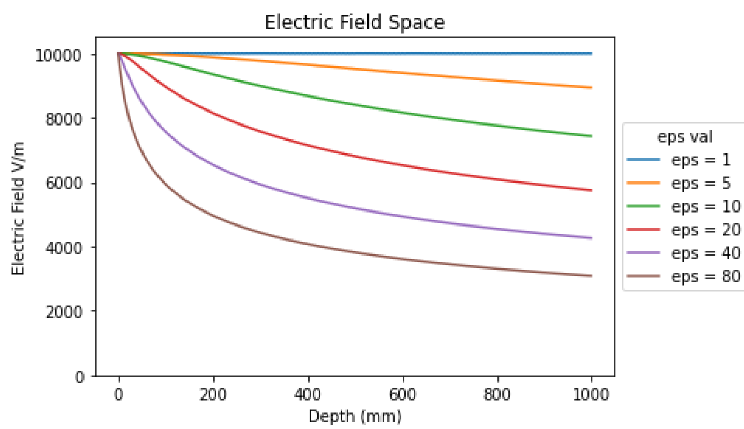

Figure 4.2. Tuning Permittivity Values with Static μ_r = 1 and $\sigma = 0$ (1000 mm)

Permeability value variation do not as significantly affect electric field for most expected values, as illustrated in Figure 4.3. In the range of expected values for actual materials, the μ_r values will not be the driving force for decreasing the overall electric field, as permeability within the most common range decreases the electric field by less than 10% of the original electric field. That said, the materials of focus tended to be non-metallic, which significantly restricted the expected range for permeability.

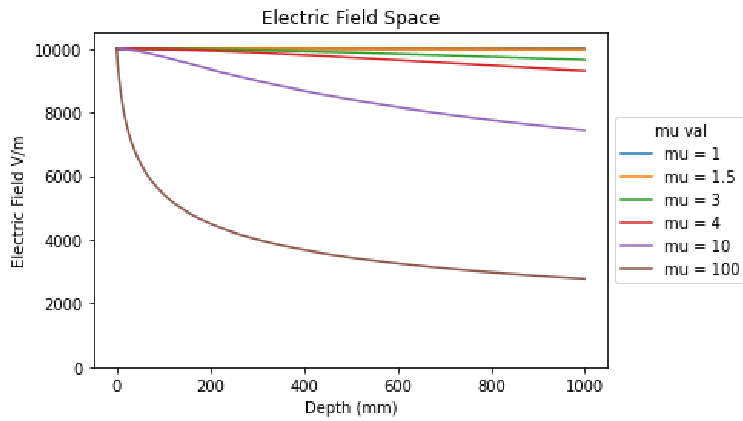

Figure 4.3. Tuning Permeability Values with Static $\varepsilon_r = 1$ and $\sigma = 0$ (1000 mm)

In addition to examining the attenuation of the field over space, we can plot the trend in the resulting field at a given depth. In this, we ran the same type of simulation with a range of material values, then plotted the field values at a given depth as the parameter was increased. From this, we calculated regression analysis to characterize the trend in the modeled space with the expectation that a regression curve could approximate the expected field value at a given depth.

Figure 4.4 shows the value of the electric field at specific depths for a range of electrical conductivity values. It was generated by taking each value of σ^e at intervals of 0.005 in the range of $[0, 0.1]$. Each marker represents values of the field at either the 250mm or 1000mm depth at equally spaced points. When tuning the electrical conductivity, we see a very fast drop off in the electric field strength at given depths. The point corresponding to $\sigma^e = 0$ shows no significant attenuation at any depth, but increasing the value affects the propagation very quickly, which aligns with the trend seen in Figure 4.1.

By conducting both polynomial and exponential regression, we see the best fit to the conductivity via exponential regression, which aligns with frequency-based analysis of wave propagation., but see less accuracy at full depth or at the edge of the penetration. We see in (4.1) that the constant intercept term for the regression shows large deviation from the initial field applied, indicating the quadratic model would not be viable for predicting effects of small conductivity inputs at the 1000mm depth and that a higher degree polynomial would be necessary to appropriately predict the trend at this depth. It also highlights the

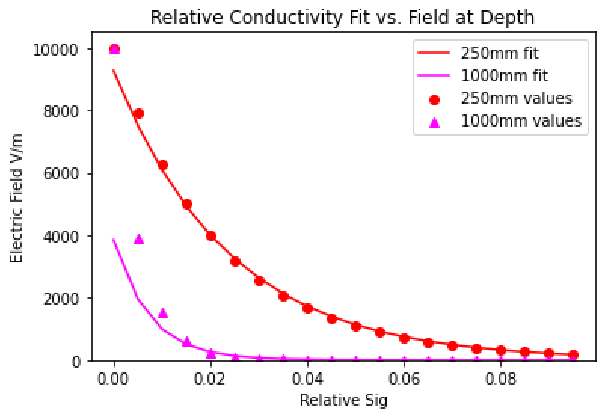

Figure 4.4. Comparing Conductivity with Depth (Varied Depth)

diminishing return of increasing conductivity values as the depth increases.

$$
\begin{aligned}
250 : E_{max} &= 9262.88e^{-41.92\sigma} \\
1000 : E_{max} &= 3846.33e^{-135.12\sigma}
\end{aligned}
\tag{4.1}
$$

Figure 4.5 provides similar visualization for adjusting the permittivity values in the range $[0, 100]$ at intervals of five. The points indicate the curve representing this relationship is beginning to approach horizontal, which would point to there being diminishing returns on increasing an object's permittivity for wave attenuation.

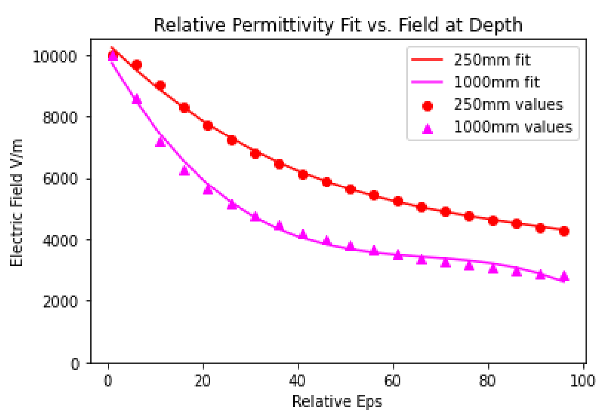

Figure 4.5. Comparing Permittivity with Depth (Varied Depth)

By conducting regression on the permittivity relationship, we observe a relationship that is best approximated by a cubic curve for the specified range of permittivity values. Although higher values of ε would likely deviate from this curve, these values would be outside the expected range for any material used in construction projects.

$$\begin{aligned} 250 : E_{max} &= -.005\varepsilon^3 + 1.4\varepsilon^2 - 152.1\varepsilon + 10376.1 \\ 1000 : E_{max} &= -.020\varepsilon^3 + 3.9\varepsilon^2 - 273.2\varepsilon + 10001.9 \end{aligned} \tag{4.2}$$

Figure 4.6 shows a similar trend for the variation of the permeability in materials, although the shape of the curve differs. The curve when varying μ does not appear to approach a horizontal asymptote in this figure but would likely approach a diminishing return based on 4.3. The lack of this shape is likely due to the low expected permeability values in non-metals, which constituted the main portion of tested parameters.

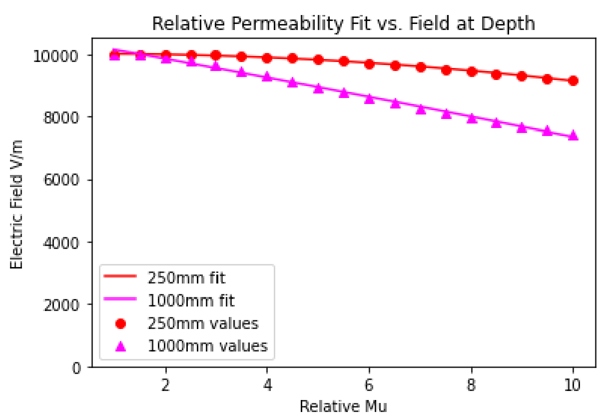

Figure 4.6. Comparing Permeability with Depth (Varied Depth)

Similar to above, we see that quadratic regression provides a tool for examining permeability value variation. What we see in (4.3) is the coefficient of the leading term is negative. This indicates that at these range of values of μ there is not a decreasing return on increasing the parameter. However, the range tested on permeability is smaller than in permittivity, meaning the values may have not reached the level of diminishing returns.

$$\begin{aligned} 250 : E_{max} &= -9.65\mu^2 + 9.28\mu + 10012.02 \\ 1000 : E_{max} &= -1.75\mu^2 - 292.20\mu + 10445.57 \end{aligned} \tag{4.3}$$

When examining the polynomial regression on these, curves, it is important to recognize the predictor is only valid for the modeled depth.

One point to note is the potential error numerical dispersion in FDTD methods and their influence on parameter importance [42]. Specifically, the ε and μ variables are susceptible to this, as the wave input to the system was narrow when compared to the spatial step size.

4.2 Tuning spatial and Temporal Parameters

Grid structure analysis was conducted by varying the values of Δx and Δt such that (3.24) is satisfied. To test and validate this in materials, a reference material with $\varepsilon_r = 3$, $\mu_r = 3$, and $\sigma^e = .03$ was used to test attenuation. These values provide a numerically viable starting point since $v = \frac{1}{\sqrt{3*\varepsilon_0*3*\mu_0}} \approx 10^8$. This value allows test of Δx and Δt that differ by at least eight orders of magnitude. For experimentation, these values were coupled and so that their ratio was on the order of 10^8, along with the base case developed for free space.

The first item of note is that the rates of convergence do differ between differing step sizes. When examining Figure 4.7, we observe the parameters with the smallest step size show the same rate of attenuation. The larger step sizes show a faster rate of decrease, indicating a larger error term affecting the calculated value. That said, all these variations converge to within .165% of the starting field values within our test range.

4.3 Threshold Values

Since this model works most effectively at evaluating attenuation of waves as they propagate through the material, tests were run on specific materials to find thresholds of field decrease. Below a layer of the construction material of concrete, the natural barriers of clay and limestone, and an underwater venue were tested as potential protective layers.

Table 4.1 reinforces the previously found relationships between material parameters as

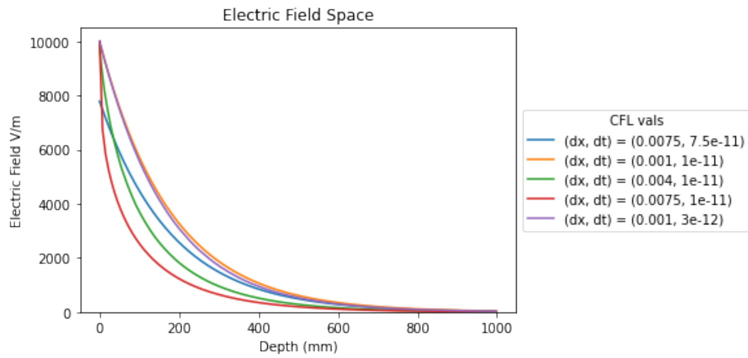

Figure 4.7. Tuning the Temporal and spatial Steps with Constant Material (1000 mm)

related to attenuation. The conductivity is by far the most significant factor to affect when the field decreases to the specified threshold. Of the solid materials, concrete showed the best rate of attenuation. This intuitively holds, as it has relatively high values of each material parameter. We also see that the distance to decrease field magnitudes increases as the threshold value is tightened. This aligns with the asymptotic behavior seen in the spatial charts in Section 4.1.

Table 4.1. Material Threshold Depths

Depth of Threshold					
ε_r / μ_r / σ^e	10%	1%	0.1%	0.01%	0.001%
4 / 4 / .1 Concrete	119mm	241mm	390mm	1206mm	2447mm
20 / 1 / .01 Clay	2245mm	8175mm	13299mm	18538mm	23843mm
6 / 1 / .2 Limestone	155mm	311mm	580mm	1809mm	5713mm
73 / 1 / 4.8 Sea Water	22mm	46mm	118mm	369mm	785mm

4.4 Non-Homogeneous Layering

Since it would be very uncommon to have a perfectly homogeneous material, we developed and ran a set of parameters for a dual property material and compared it with the boundaries expected of its constituent properties. We used properties of dry and moist sandy soil to examine the trend for a continuous function and jump discontinuity of the properties.

As seen in Figure 4.8, non-homogeneity provides additional benefit over a homogeneous layer with a higher value of ε_r. The reason for the improved values is due to reflection at each boundary when the permittivity in the new layer is higher. At each change in ε_r, a portion of the propagating field is reflected back.

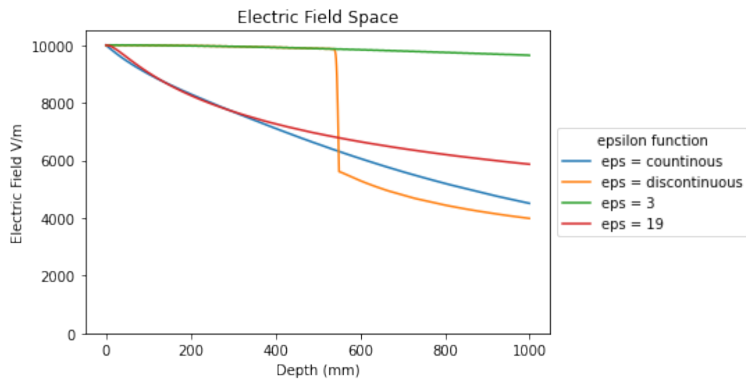

Figure 4.8. Wave Penetration with Non-Static Permittivity (1000 mm)

The magnitude of the reflection is a function of the relative permittivities as given by [43]:

$$r = \frac{(\varepsilon_{r1} - \varepsilon_{r2})^2}{(\varepsilon_{r1} + \varepsilon_{r2})^2} \tag{4.4}$$

This gives the percent of the wave reflected at any interface between materials. This explains the large decrease in the jump discontinuity, where approximately 53% of the wave is reflected. We also see much steeper descent in the rate of attenuation in the material where the permittivity varies as a function of space. At each step of the discretization, approximately .02% of the wave is reflected. This magnitude of reflection varies and is slightly larger at the beginning, eventually flattening as the $(\varepsilon - \Delta x)$ the value of the largest value of ε.

4.5 Metamaterials

There is a special subset of artificially designed materials that have negative values for both ε and μ [44]. We examined these metamaterials to see if they have application in EMP shielding along with other known applications in electronic systems.

For testing the effect of σ^e, we used nominal values that would demonstrate variation. We observe in Figure 4.9 that sigma significantly affects metamaterials in the opposite manner as traditional materials. In the base case of $\sigma^e = 0$, we see expected deterioration of the electric field. Unlike traditional materials, we see a sharp decrease in the shielding effect with the increase in permittivity. Due to the mechanism for propagation and the deliberate construction of metamaterials, the metamaterials act as an amplifier when the conductivity is high.

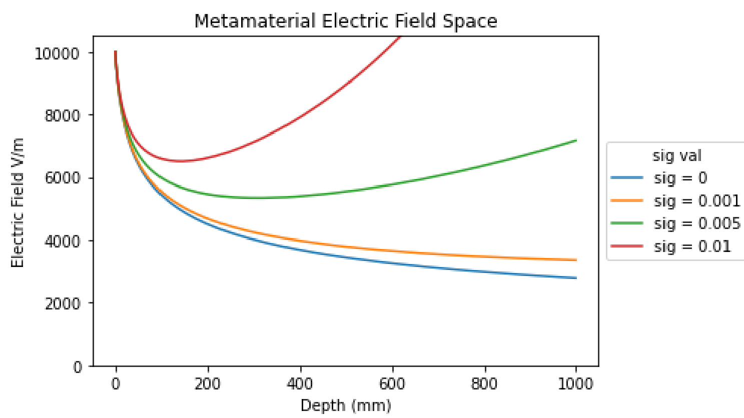

Figure 4.9. Tuning Conductivity Values with Static $\varepsilon_r = -10$ and $\mu_r = -10$ (1000 mm)

Looking at coupled variations on the ε_r and μ_r values, we observe in Figure 4.10 that the permittivity values have more effect than the permeability values with the presence of a conductivity value.

We observe in Figure 4.11 that the metamaterials offer less shielding than traditional materials with the same magnitude of permittivity and permeability. As noted in Figure 4.9, conductivity values inhibit the ability of metamaterials to reduce electric fields, and thus have higher field values at exit.

4.6 Waveform Variation

For all the previous calculations, we used a Gaussian waveform where the value of n in (3.23) is two. Differing the values of n in this equation offer analysis with waveforms of

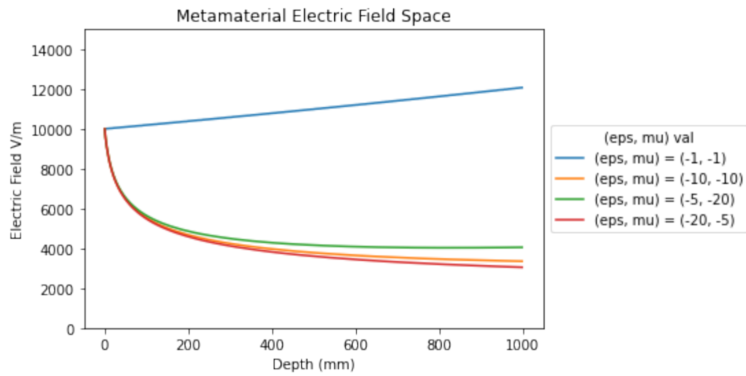

Figure 4.10. Tuning Permeability and Permittivity Values with σ^e = .001 (1000 mm)

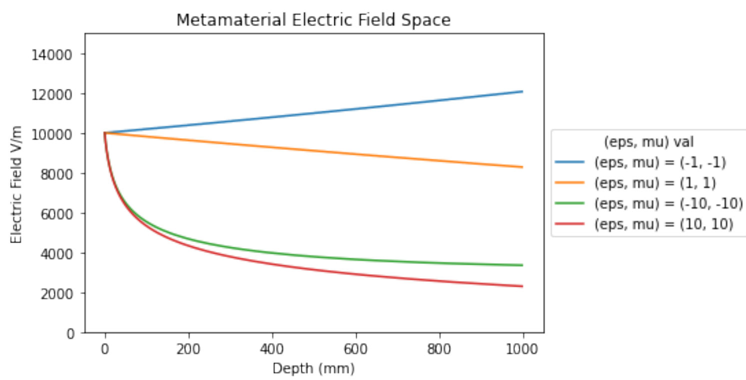

Figure 4.11. Comparing Positive and Negative Parameters with σ^e = .001 (1000 mm)

slightly varying shapes. As the value of n increases, the width of the wave increases.

As can be seen in Figure 4.12, the effects of sub and super-Gaussian waves are not significant over the depth tested. We do see slower rates of attenuation with the super-Gaussian wave, which is expected due to the wider wave containing more energy to attenuate. Although these waveforms have slightly different rates of attenuation, all the iterations have peak values at the end within .05% of the original wave magnitude.

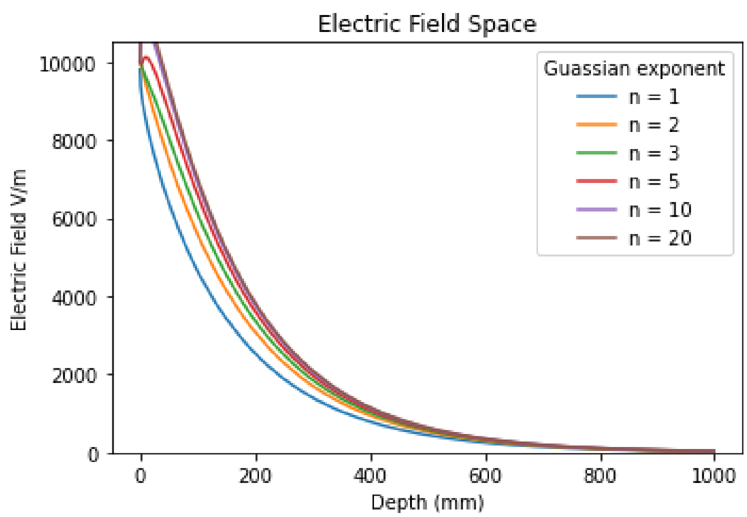

Figure 4.12. Attenuation Relationship to Waveform Value (1000 mm)

THIS PAGE INTENTIONALLY LEFT BLANK

CHAPTER 5:
Conclusion and Further Study

5.1 Conclusions

We can see that the use of construction and earthen materials does offer potential for acting as a passive protector by reducing the magnitude of the electric field from an E1 HEMP event. That said, specific thresholds may require deep layers to adequately protect, meaning that simply placing an electronic system underground would not protect a finely sensitive system without additional protection via other measures. We can summarize the key takeaways as:

- Within a normal range of values, electrical conductivity is the parameter that most affects the attenuation of the field, followed by permittivity, and finally permeability
- The calculated field will converge with altered CFL parameters so long as $\Delta t \leq \Delta x \times \sqrt{\varepsilon\mu}$
- Concrete and limestone offer protection that attenuates the field by $> 99.9\%$ at 1000mm, but not every earthen material can replicate this
- Non-homogeneous layers can provide additional protection by adding reflection to attenuation
- Metamaterials do not indicate suitability as a shield layer from electric field propagation
- Variations in the electric field waveform do not significantly affect the expected attenuation of the field

Specific tuning of parameters and depth would be dependent on the electronic system being protected and the expected blast magnitude. Since nominal values were used in this analysis, the specific level of protection could not be calculated for any given event, but trends were determined for types of materials. Once the wave enters the protective layer, we found that electric conductivity is by far the most significant material property for reducing electric field propagation.

Overall, E1 HEMP protection is a complex environment that requires many assumptions due to the lack of available specific details. That said, we can perform behavior analysis and see the types of capabilities that would offer a level of passive protection from the peak damage by electric field propagation. This document presents baseline details on the interaction of the varied components that affect wave attenuation and offers a starting point for expanded analysis of protective measures.

5.2 Further Study

There are multiple directions to extend this solution set, chiefly in the solving technique and the parameters of the problem. Addition differential solvers offer validation and opportunity to improve efficiency in larger spaces. Parameter extension offers opportunity to examine the effects in higher dimensions and with more complex material property arrangements.

When looking at further solving methods, Galerkin methods and finite volume solvers offer good directions of validation and expansion on this work. These solving methods can be used in conjunction with experimental testing to shape solving environments for larger scale problem sets. Additionally, to improve performance, expansion to programming languages tuned toward scientific computing provide a method to expand the problem space in calculations.

To provide a more robust picture of attenuation, this problem can also be solved in higher dimensions. The natural next step is a 2-D and 3-D extensions in the Cartesian plane. The equations in (3.9) offer the starting point for discretization along the generalized version of the Yee grid. Appropriate simplifications and discretizations can then be used to model the higher dimensional problem in the same manner as the 1-D case. This higher dimension case also offers the first opportunity to use materials with anisotropic dielectric properties corresponding to each directional component. Additionally, further testing should examine numerical dispersion within the system and test differing widths for wave forms interacting with the media.

Further material expansion provides an additional direction of study. Interactions and ordering of composite barriers can provide a more comprehensive picture of the preferred materials for HEMP protection. Including open air as a layer could provide a more robust indication of behavior by including reflection of waves reaching the boundary layer, as the current model uses a nominal value entering the layer rather than a nominal value hitting the layer. Additionally, since metals have extremely high permittivity values, they could offer additional parameter examination and layering options. These differences could indicate the role of material ordering in passive EMP protections.

THIS PAGE INTENTIONALLY LEFT BLANK

APPENDIX: FDTD Python Code

```
def oneD_FDTD(re=1, sig=0, rm=1, init=1e4, depth=1, dx=1e-3, dt=3e-12, n=2):

    '''
    Single Material FDTD
    Runs the finite element calculation for propagation of electic and magnetic fields through a
    material in one dimension for a homogeneous material.  It then stores and returns maximum field
    values in spacial and temporal directions.  This code is designed for a single material at a
    specified depth. It calculates the time for the front edge of a EM wave to penetrate to the
    depth, and simulates that many steps.

    Inputs:
    re     : relative permittivity
    sig    : electrical conductivity
    rm     : relative permeability
    init   : initial electric field value
    depth  : thickness of material in meters
    dx     : size of spatial step
    dt     : size of temporal step
    n      : exponent of Guassian waveform function

    Simulation Properties
    depth: thickness of material in meters
    time steps: how many picoseconds run
    init: initial electic field
    '''

    eps_0 = 8.854187817e-12         # free space permittivity
    mu_0 = 1.256637061e-6           # free space permeability

    m_sig = 0                       # always zero for non-magnetic system

    eps = eps_0 * re                # permittivity in this material
    mu  = mu_0 * rm                 # permeability in this material

    # Speed of waves in the medium
    v = 1/math.sqrt(mu*eps)         # speed of light in the medium

    # Number of steps in space
    nx = math.floor(depth/dx)+200       # number of cells in 1D problem space

    # Time to fully penetrate
    steps = round(((nx-200)*depth * dx) / (v * dt))+200

    # Initialize field and material arrays
    Ce1       = np.zeros(nx+1)
    Ce2       = np.zeros(nx+1)
```

```
Ce3        = np.zeros(nx+1)
E          = np.zeros(nx+1)
Jz         = np.zeros(nx+1)
eps        = eps*np.ones(nx+1)
sigma_e    = sig*np.ones(nx+1)

Ch1        = np.zeros(nx);
Ch2        = np.zeros(nx);
H          = np.zeros(nx);
mu         = mu*np.ones(nx);         # Doesn't have to be uniform, can be
sigma_m    = m_sig*np.ones(nx);      # like above, based on values from above

# Calculate update coefficients
# Electric
Ce1 = np.multiply((2*eps - dt*sigma_e), 1/(2*eps + dt*sigma_e))
Ce2 = np.multiply((2*dt/dx), 1/(2*eps + dt*sigma_e))
Ce3 = np.multiply((-2*dt),1/(2*eps + dt*sigma_e))
# Magnetic
Ch1 = np.multiply((2*mu - dt*sigma_m),1/(2*mu + dt*sigma_m))
Ch2 = np.multiply((2*dt/dx),1/(2*mu + dt*sigma_m))


## Define the Gaussian source waveform
time = dt*np.arange(steps)
Jz_waveform =  init * np.exp(-abs(((time-2e-10)/5e-11))**n)  # Used to simulate electric
                                                             # field coming as wave

# Electric field entering boundary
E[0] = Jz_waveform[0]                 # First value in waveform corresponds to leading edge
                                      # of E field

pen  = round(1/dx * (v * dt * steps))     # depth penetration calculation in mm

mag_store = np.zeros(steps)
mag_space = np.zeros(nx)
ele_store = np.zeros(steps)
ele_space = np.zeros(nx+1)

tot1 = np.arange(steps)
tot2 = np.arange(nx)
tot3 = np.arange(pen)


for time_step in tot1:
    # update Jz for the current time step (unneeded unless adding induced wave internal)
    #Jz[Ji_index] = Jz_waveform[time_step]

    # update magnetic field
    H=np.multiply(Ch1,H)+np.multiply(Ch2,E[1:nx+1]-E[0:nx])
```

```
    # update electric field
    E[1:nx] = np.multiply(Ce1[1:nx],E[1:nx])+np.multiply(Ce2[1:nx],H[1:nx] - H[0:nx-1])
                                    #+np.multiply(Ce3[1:nx],Jz[1:nx]) # Zero unless inducing

    # Store max values in each propagating field (time-wise)
    mag_store[time_step] = np.amax(abs(H))
    ele_store[time_step] = np.amax(abs(E))

    # Store max values in each propagating field (space-wise)
    mag_space = np.maximum(mag_space, abs(H))
    ele_space = np.maximum(ele_space, abs(E))

    E[0]=Jz_waveform[time_step]

mag_store = np.around(mag_store, 10) # Rounds decimal to 10 places
ele_store = np.around(ele_store, 10) # Keeps from storing values below accuracy
mag_space = np.around(mag_space, 10)
ele_space = np.around(ele_space, 10)

print('Max E field at the end of the time simulation is %.4e V/m' %(ele_store[-100]))

return ele_space, pen #mag_store, ele_store, mag_space
```

THIS PAGE INTENTIONALLY LEFT BLANK

List of References

[1] C. Wilson, “High altitude electromagnetic pulse (HEMP) and high power microwave (HPM) devices: threat assessments,” Library of Congress, Washington DC: Congressional Research Service, Tech. Rep., 2004.

[2] C. Wilson, “High altitude electromagnetic pulse (HEMP) and high power microwave (HPM) devices: threat assessments,” Library of Congress, Washington DC: Congressional Research Service, Tech. Rep., 2008.

[3] W. House. (2019). Executive Order on Coordinating National Resilience to Electromagnetic Pulses. [Online]. Available: https://www.federalregister.gov/documents/2019/03/29/2019-06325/coordinating-national-resilience-to-electromagnetic-pulses

[4] E. Savage, J. Gilbert, and W. Radasky, “The early time (E1) high-altitude electromagnetic pulse (HEMP) and its impact on the US power grid,” *Report Meta-R-320 for Oak Ridge National Laboratory*, 2010.

[5] J. S. Foster Jr, M. E. Gjelde, W. R. Graham, R. J. Hermann, M. H. H. M. Kluepfel, G. K. Soper, and L. L. Wood Jr, “Report of the commission to assess the threat to the United States from electromagnetic pulse (EMP) attack,” *Critical National Infrastructures Report*, vol. 1, 2004.

[6] W. J. Broad, “Nuclear pulse (iii): Ensuring delivery of the doomsday signal,” *Science*, vol. 212, no. 4500, pp. 1248–1251, 1981.

[7] C. E. Baum, “From the electromagnetic pulse to high-power electromagnetics,” *Proceedings of the IEEE*, vol. 80, no. 6, pp. 789–817, 1992.

[8] C. N. Vittitoe, “Did high-altitude EMP (electromagnetic pulse) cause the Hawaiian streetlight incident,” Sandia National Labs, Tech. Rep., 4 1989. Available: https://www.osti.gov/biblio/6151435

[9] C. Longmire, “EMP on Honolulu from the Starfish Event,” *US Air Force Weapons Laboratory Theoretical Note*, vol. 353, 1985.

[10] W. J. Broad, “Nuclear pulse (i): Awakening to the chaos factor,” *Science*, vol. 212, no. 4498, pp. 1009–1012, 1981.

[11] S. J. Chapman, D. P. Hewett, and L. N. Trefethen, “Mathematics of the Faraday cage,” *SIAM Review*, vol. 57, no. 3, pp. 398–417, 2015.

[12] C. L. Longmire, R. M. Hamilton, and J. M. Hahn, “A nominal set of high-altitude EMP environments,” Oak Ridge National Laboratory, Tech. Rep., 2 1987. Available: https://www.osti.gov/biblio/7096596

[13] W. Karzas and R. Latter, “Detection of the electromagnetic radiation from nuclear explosions in space,” *Physical Review*, vol. 137, no. 5B, p. B1369, 1965.

[14] D. of Defense, “The Militarily Critical Technologies List Part II: Weapons of Mass Destruction Technologies,” Department of Defense, Tech. Rep. ADA 330102, 1998.

[15] A. Taflove and S. C. Hagness, *Computational electromagnetics: the finite-difference time-domain method*. London, UK: Artech House, 2000.

[16] S. D. Gedney, *Introduction to the Finite-Difference Time-Domain (FDTD) Method for Electromagnetics*. San Rafael, CA: Morgan & Claypool Publishers, 2011.

[17] T. Weiland, “A discretization model for the solution of Maxwell’s equations for six-component fields,” *Archiv Elektronik und Uebertragungstechnik*, vol. 31, pp. 116–120, 1977.

[18] Product platform: COMSOL multiphysics. (n.d.). COMSOL. [Online]. Available: https://www.comsol.com/comsol-multiphysics. Accessed Apr. 13, 2021.

[19] A. Z. Elsherbeni and V. Demir, *The Finite-Difference Time-Domain Method for Electromagnetics with MATLAB Simulations*, 2nd ed. (Electromagnetics and Radar). Edison, NJ: SciTech Publishing, 2016.

[20] K. Yee, “Numerical solution of initial boundary value problems involving Maxwell’s equations in isotropic media,” *IEEE Transactions on antennas and propagation*, vol. 14, no. 3, pp. 302–307, 1966.

[21] R. Holland, “THREDE: a free-field EMP coupling and scattering code,” *IEEE Transactions on Nuclear Science*, vol. 24, no. 6, pp. 2416–2421, 1977.

[22] R. Holland, “THREDS: a finite-difference time-domain EMP code in 3D spherical coordinates,” *IEEE Transactions on Nuclear Science*, vol. 30, no. 6, pp. 4592–4595, 1983.

[23] R. Courant, K. Friedrichs, and H. Lewy, “On the Partial Difference Equations of Mathematical Physics,” *IBM journal of Research and Development*, vol. 11, no. 2, pp. 215–234, 1967.

[24] J. A. Stratton, *Electromagnetic Theory*. New York City, NY: McGraw-Hill, 1941.

[25] J. Stewart, *Calculus: Early Transcendentals*, 8th ed. Boston, MA: Cengage Learning, 2016.

[26] M. Mojahedi. ECE1228 Course Notes. University of Toronto. [Online]. Available: https://www.waves.utoronto.ca/prof/mojahedi/ECE1228/Course%20Notes%20Set%201.pdf

[27] J. Smith. (2010). *Physical Audio Signal Processing*. [Ebrary version]. [Online]. Available: http://ccrma.stanford.edu/~jos/pasp/

[28] U. M. Ascher and C. Greif, *A first Course on Numerical Methods*. Philadelphia, PA: SIAM, 2011.

[29] L. Weinstein, *Electromagnetic Waves*. Moscow, RU: Radio i svyaz', 1988.

[30] Magnetic reluctance: what is it? (formula, units & applications). (2020). Electrical4U. [Online]. Available: https://www.electrical4u.com/magnetic-reluctance/. Accessed Apr. 21, 2021.

[31] Table of electrical resistivity and conductivity. (n.d.). *ThoughtCo*. [Online]. Available: https://www.thoughtco.com/table-of-electrical-resistivity-conductivity-608499. Accessed Apr. 09, 2021.

[32] S. S. Hubbard, J. E. Peterson, E. L. Majer, P. T. Zawislanski, K. H. Williams, J. Roberts, and F. Wobber, "Estimation of permeable pathways and water content using tomographic radar data," *The Leading Edge*, vol. 16, no. 11, pp. 1623–1628, 11 1997.

[33] D. G. Archer and P. Wang, "The dielectric constant of water and debye hückel limiting law slopes," *Journal of Physical and Chemical Reference Data*, vol. 19, no. 2, pp. 371–411, 1990.

[34] R. Lang, Y. Zhou, C. Utku, and D. Le Vine, "Accurate measurements of the dielectric constant of seawater at l band," *Radio Science*, vol. 51, no. 1, pp. 2–24, Jan. 2016.

[35] J. Davis, Y. Huang, S. Millard, and J. Bungey, "Determination of dielectric properties of in situ concrete at radar frequencies," *Non-Destructive Testing in Civil Engineering*, 2003.

[36] J. H. Scott, "Electrical and magnetic properties of rock and soil," US Geological Survey, Tech. Rep., 1983.

[37] E. Toolbox. (2010). Relative Permittivity - the Dilectric Constant. [Online]. Available: https://www.engineeringtoolbox.com/relative-permittivity-d_1660.html. Accessed Feb. 21 , 2021.

[38] G. Elert. (2021). *The Physics Hypertextbook*. [Online]. Available: https://physics.info/dielectrics/. Accessed Apr. 09, 2021.

[39] L. Mari. (2020, 08). An introduction to soil resistivity. EE Power. [Online]. Available: https://eepower.com/technical-articles/an-introduction-to-soil-resistivity/#

[40] B. Notaros, *MATLAB-Based Electromagnetics*. New York City, NY: Pearson Higher Ed, 2013.

[41] J. Jackson, *Classical Electrodynamics*, 3rd ed. Wiley, 1998.

[42] J. Juntunen and T. Tsiboukis, “Reduction of numerical dispersion in fdtd method through artificial anisotropy,” *IEEE Transactions on Microwave Theory and Techniques*, vol. 48, no. 4, pp. 582–588, 2000.

[43] F. W. Sears, *Electricity and Magnetism*. Boston, MA: Addison-Wesley, 1951.

[44] J. Li and Y. Huang, *Time-Domain Finite Element Methods for Maxwell’s Equations in Metamaterials*. New York City, NY: Springer, 2013.

Initial Distribution List

1. Defense Technical Information Center
   Ft. Belvoir, Virginia

2. Dudley Knox Library
   Naval Postgraduate School
   Monterey, California